

# Acoustic Vector-Sensor Correlations in Ambient Noise

Malcolm Hawkes, *Member, IEEE* and Arye Nehorai, *Fellow, IEEE*

**Abstract**—Most array-processing methods require knowledge of the correlation structure of the noise. While such information may sometimes be obtained from measurements made when no sources are present, this may not always be possible. Furthermore, measurements made *in-situ* can hardly be used to analyze system performance before deployment. The development of models of the correlation structure under various environmental assumptions is therefore very important. In this paper, we obtain integral and closed form expressions for the auto- and cross-correlations between the components of an acoustic vector sensor (AVS) for a wideband-noise field, under the following assumptions concerning its spatial distribution: 1) azimuthal independence; 2) azimuthal independence and elevational symmetry; and 3) spherical isotropy. We also derive expressions for the cross-covariances between all components of two spatially displaced AVSs in a narrowband-noise field under the same assumptions. These results can be used to determine the noise-covariance matrix of an array of acoustic vector sensors in ambient noise. We apply them to a uniform linear AVS array to assess its beamforming capabilities and localization accuracy, via the Cramér–Rao bound, in isotropic and anisotropic noise.

**Index Terms**—Acoustic vector sensor, ambient noise, anisotropic noise, array processing, noise correlation.

## I. INTRODUCTION

ACOUSTIC vector sensors (AVSs) measure the acoustic pressure and all three orthogonal components of the acoustic particle velocity at a single point in space. These sensors, and arrays composed of them, have a number of advantages over traditional hydrophone arrays [1]–[5], for example, improved performance for a given aperture; full azimuth/elevation estimation with a linear array (or even a single AVS), e.g., they do not suffer from the well-known left/right ambiguity that occurs in towed array scenarios; and they can be used in a sparse (undersampled) configuration with *uniform* geometry. Much work is currently being done on the development of velocity sensors [6] and complete vector sensors have already been constructed and tested at sea [7], [8].

The performance results in [1]–[5], as well as direction estimation algorithms that have been proposed for AVSs [2], [3], [9]–[12], all assume that the noise is uncorrelated

between different sensor components within a single vector sensor, and between all components of two vector sensors at different locations, i.e., with a slight abuse of language, it is spatially white. Such an assumption is required by most sensor-array-processing methods [13] and implies that either the noise is truly spatially white, or that the data are processed so as to *pre-whiten* the noise. The former is generally only valid for internal sensor noise, which is not the major noise source in practical systems, while the latter requires that the noise covariance be known up to a multiplicative constant. While this information may sometimes be obtained from measurements made when no sources are present, this may not always be possible. Furthermore, measurements made *in-situ* can hardly be used to analyze system performance before deployment. Finally, knowledge of how an array will perform in a given noise environment is very important for array design. Since alterations in an array's geometry after deployment is generally impractical, the design process must be carried out using noise statistics based on mathematical models of the ocean environment. Therefore, the development of models of the correlation structure under various environmental assumptions is very important. Some authors have considered ways to circumvent the requirement for complete knowledge of the noise-correlation structure without resorting to higher-order statistics e.g., [14] and [15]. These methods typically parameterize the noise as a linear combination of known matrices obtained based on *a-priori* knowledge including ambient-noise models. The results presented in this paper lead to highly structured-noise covariance matrices that can be used in such noise models.

Numerous papers have considered the spatial correlation of the ambient pressure field, the results of which are applicable to traditional (scalar) hydrophone arrays, under various assumptions on the distributions of noise sources and the propagation environment [16]–[21], resulting in isotropic and various anisotropic models. In this paper, we investigate the spatio-temporal correlation of a vector sensor array under various ambient-noise conditions. We suppose that the noise field is made up of uncorrelated propagating planewaves from all possible directions, i.e., it is homogeneous. We obtain integral and closed-form expressions for the auto- and cross-correlations between the components of a single acoustic vector sensor for a wideband-noise field, under the following assumptions concerning its spatial distribution: 1) azimuthal independence; 2) azimuthal independence and elevational symmetry; and 3) spherical isotropy. We also derive expressions for the cross-covariances between all components of two spatially displaced AVSs in a narrowband-noise field under the same assumptions. These results can be used to determine the structure

Manuscript received June 30, 2000; revised April 9, 2001. This work was supported in part by the Air Force Office of Scientific Research under Grant F49620-97-1-0481 and Grant F49620-99-1-0067, in part by the Office of Naval Research under Grant N 00014-981-0542, and in part by the National Science Foundation under Grant MIP-9615590.

M. Hawkes was with the Department of Electrical Engineering and Computer Science, University of Illinois, Chicago, IL 60607 USA. He is now with Stafford Trading Inc., Chicago, IL 60604 USA.

A. Nehorai is with the Department of Electrical Engineering, University of Illinois, Chicago, IL 60607 USA.

Publisher Item Identifier S 0364-9059(01)07215-6.

of the noise covariance of an AVS array under a given ambient-noise model. For example, it is shown that, unlike its pressure-sensor counterpart, a half-wavelength spaced uniform linear array of AVSs in spherically-isotropic noise does not possess a spatially white covariance matrix. We use our results to examine the localization accuracy of a linear AVS array in isotropic and anisotropic noise fields using the Cramér–Rao bound. A number of interesting phenomena are observed. For example, the direction, estimation, and beamforming capabilities are better for many source directions in an ambient-noise field than in spatially white noise and, in ambient noise, the source locations that can be estimated most accurately are not always those near broadside. The performance is compared with previous results on the CRB and beamforming performance of an AVS array that assumed spatially white noise [3], [4], and with a standard pressure-sensor array. The effect of the ambient-noise field on a conventional beamformer is also investigated.

This work extends [22], which computed the within-sensor covariance matrix of a single AVS, and [23], which derived cross-correlations of the velocity field. Both papers assumed narrowband spherically-isotropic noise. The results presented here will be useful for predicting the performance of AVS arrays in realistic ambient-noise-limited scenarios and consequently, for system evaluation and design. Furthermore, they provide *a-priori* knowledge that can be used to obtain accurate estimated-noise covariances or to provide a basis for a parametric-noise model, to use in processing algorithms.

In Section II, we develop the noise and measurement models. In Section III, the within-sensor correlations, i.e., the covariance matrix of the output of a single vector sensor, is considered and Section III-A deals with the cross-covariances between two spatially separated vector sensors. In Section IV we examine the CRB and conventional beamformer for an AVS array in isotropic and anisotropic ambient noise and provide a detailed discussion of the results. Section V concludes the paper.

## II. NOISE AND MEASUREMENT MODELS

We suppose that the noise field can be expressed as a superposition of propagating plane waves from all possible directions, i.e., the pressure at location  $\mathbf{r}$  and time  $t$  is

$$p(\mathbf{r}, t) = \int_{\mathcal{U}} p_{\mathbf{u}}(t + \mathbf{u}^T \mathbf{r}/c) d\mathbf{u} \quad (1)$$

where

- $\mathbf{u}$  three-dimensional unit-length vector;
- $\mathcal{U}$  surface of the unit sphere;
- $d\mathbf{u}$  elemental area with outward normal  $\mathbf{u}$ ;
- $c$  speed of sound;
- $p_{\mathbf{u}}(t)$  acoustic pressure at the origin resulting from the planewave arriving from direction  $\mathbf{u}$ .

The acoustic velocity associated with each planewave is given by Euler's equation [24]

$$\mathbf{v}_{\mathbf{u}}(t + \mathbf{u}^T \mathbf{r}/c) = -\mathbf{u} p_{\mathbf{u}}(t + \mathbf{u}^T \mathbf{r}/c)/\rho c \quad (2)$$

and the resultant velocity field is

$$\begin{aligned} \mathbf{v}(\mathbf{r}, t) &= \int_{\mathcal{U}} \mathbf{v}_{\mathbf{u}}(t + \mathbf{u}^T \mathbf{r}/c) d\mathbf{u} \\ &= -\frac{1}{\rho c} \int_{\mathcal{U}} \mathbf{u} p_{\mathbf{u}}(t + \mathbf{u}^T \mathbf{r}/c) d\mathbf{u}. \end{aligned} \quad (3)$$

If each planewave is band limited,  $p_{\mathbf{u}}(t) = \Re\{\tilde{p}_{\mathbf{u}}(t)e^{-i\omega_c t}\}$ , where  $\tilde{p}_{\mathbf{u}}(t)$  is the complex envelope of  $p_{\mathbf{u}}(t)$  and  $\omega_c$  is the center frequency. Then

$$p(\mathbf{r}, t) = \Re\{\tilde{p}(\mathbf{r}, t)e^{-i\omega_c t}\} \quad (4)$$

$$\mathbf{v}(\mathbf{r}, t) = \Re\{\tilde{\mathbf{v}}(\mathbf{r}, t)e^{-i\omega_c t}\} \quad (5)$$

where the complex envelopes are

$$\tilde{p}(\mathbf{r}, t) = \int_{\mathcal{U}} \tilde{p}_{\mathbf{u}}(t + \mathbf{u}^T \mathbf{r}/c) e^{-i\omega_c \mathbf{u}^T \mathbf{r}/c} d\mathbf{u} \quad (6)$$

$$\tilde{\mathbf{v}}(\mathbf{r}, t) = -\frac{1}{\rho c} \int_{\mathcal{U}} \mathbf{u} \tilde{p}_{\mathbf{u}}(t + \mathbf{u}^T \mathbf{r}/c) e^{-i\omega_c \mathbf{u}^T \mathbf{r}/c} d\mathbf{u}. \quad (7)$$

The quantity measured by an acoustic-vector sensor whose velocity sensors are aligned with the coordinate axes, after normalization of the velocity measurements and conversion to baseband, is the vector  $\mathbf{y}(\mathbf{r}, t) \triangleq [y_p(\mathbf{r}, t), \mathbf{y}_v(\mathbf{r}, t)^T]^T$ , where  $y_p(\mathbf{r}, t) = \tilde{p}(\mathbf{r}, t)$  and  $\mathbf{y}_v(\mathbf{r}, t) = -\rho c \tilde{\mathbf{v}}(\mathbf{r}, t)$  (see [2]). We shall derive expressions for the covariance matrix of  $\mathbf{y}(\mathbf{r}, t)$ , i.e., the auto and cross-covariances between the components of a single vector sensor, and the cross-covariance matrix between  $\mathbf{y}(\mathbf{r}_1, t_1)$  and  $\mathbf{y}(\mathbf{r}_2, t_2)$ , i.e., the cross-correlations between the outputs of two spatially separated vector sensors at locations  $\mathbf{r}_1$  and  $\mathbf{r}_2$  and times  $t_1$  and  $t_2$ , under various assumptions regarding the spatial symmetry of the noise.

Let  $p_{\mathbf{u}}(t)$  be a zero-mean stochastic process for each  $\mathbf{u}$ . Thus  $\tilde{p}(\mathbf{r}, t)$  and  $\tilde{\mathbf{v}}(\mathbf{r}, t)$  are also zero mean stochastic processes. The cross-covariances between all planewaves contributing to the noise field are defined by

$$\tilde{R}_{\mathbf{u}_1 \mathbf{u}_2}(t_1, t_2) \triangleq E\{\tilde{p}_{\mathbf{u}_1}(t_1) \tilde{p}_{\mathbf{u}_2}^H(t_2)\}. \quad (8)$$

The spatio-temporal cross-covariance matrix between two vector sensors is

$$\begin{aligned} R(\mathbf{r}_1, \mathbf{r}_2, t_1, t_2) &\triangleq E\{\mathbf{y}(\mathbf{r}_1, t_1) \mathbf{y}^H(\mathbf{r}_2, t_2)\} \\ &= \int_{\mathcal{U}} \int_{\mathcal{U}} \tilde{R}_{\mathbf{u}_1 \mathbf{u}_2}(t_1 + \mathbf{u}_1^T \mathbf{r}_1/c, t_2 + \mathbf{u}_2^T \mathbf{r}_2/c) \\ &\quad \cdot e^{-i\omega_c(\mathbf{u}_1^T \mathbf{r}_1 - \mathbf{u}_2^T \mathbf{r}_2)/c} \begin{bmatrix} 1 \\ \mathbf{u}_1 \end{bmatrix} [1 \quad \mathbf{u}_2^T] d\mathbf{u}_1 d\mathbf{u}_2. \end{aligned} \quad (9)$$

This expression is valid when both vector sensors are aligned with the coordinate axes. If the  $3 \times 3$  orthonormal matrices  $L_1$  and  $L_2$  describe the orientation of the velocity sensor triad within each vector sensor, the spatio-temporal cross-covariance

is

$$\begin{aligned} & \mathbb{E}\{\mathbf{y}(\mathbf{r}_1, t_1)\mathbf{y}^H(\mathbf{r}_2, t_2)\} \\ &= \begin{bmatrix} 1 & 0 \\ 0 & L_1^T \end{bmatrix} R(\mathbf{r}_1, \mathbf{r}_2, t_1, t_2) \begin{bmatrix} 1 & 0 \\ 0 & L_2 \end{bmatrix}. \end{aligned} \quad (10)$$

With the assumptions that: i) planewaves from different directions are uncorrelated with each other and ii) all planewaves are (wide-sense) stationary, i.e.,  $p_{\mathbf{u}}(t)$ , is stationary for each  $\mathbf{u}$

$$\tilde{R}_{\mathbf{u}_1\mathbf{u}_2}(t_1, t_2) = \tilde{R}_{\mathbf{u}_1}(t_1 - t_2)\delta(\mathbf{u}_1 - \mathbf{u}_2) \quad (11)$$

where we have written  $\tilde{R}_{\mathbf{u}}(\tau)$  for  $\tilde{R}_{\mathbf{u}\mathbf{u}}(t + \tau, t)$ , since it is independent of  $t$ . Equation (9) becomes

$$\begin{aligned} & R(\mathbf{r}_1, \mathbf{r}_2, t_1, t_2) \\ &= \int_{\mathcal{U}} \tilde{R}_{\mathbf{u}}(t_1 - t_2 + \mathbf{u}^T(\mathbf{r}_1 - \mathbf{r}_2)/c) \\ & \cdot e^{-i\omega_c \mathbf{u}^T(\mathbf{r}_1 - \mathbf{r}_2)/c} \begin{bmatrix} 1 \\ \mathbf{u} \end{bmatrix} [1 \quad \mathbf{u}^T] d\mathbf{u} \end{aligned} \quad (12)$$

which depends on only the differences  $\mathbf{d} = \mathbf{r}_2 - \mathbf{r}_1$  and  $\tau = t_2 - t_1$ . Therefore, the vector-noise field is spatially homogeneous and temporally stationary, and we can denote its spatio-temporal correlation matrix by  $R(\mathbf{d}, \tau)$ . The assumption that ambient noise can be modeled as a linear superposition of uncorrelated plane waves is generally very satisfactory for deep water scenarios [20]. One of the first models of this sort was proposed in [16], which considered both volume and surface-noise models, and has been used in connection with a phenomenological approach to the modeling of deep water sound fields [17] and [19]. However, more recent theory [20] shows that, even in shallow water, the ambient-noise field is substantially homogeneous over a large proportion of the water column away from the boundaries. Therefore, the assumption of homogeneity is quite generally valid and imposes little restriction on the applicability of the theory herein.

### III. WITHIN-SENSOR COVARIANCE

We first consider the auto and cross-covariances of the four components of the output of a single vector sensor  $\mathbf{y}(t)$ . Setting  $\mathbf{d} = \mathbf{0}$  we have

$$\begin{aligned} R(\mathbf{0}, \tau) &= \int_{\mathcal{U}} \tilde{R}_{\mathbf{u}}(\tau) \begin{bmatrix} 1 \\ \mathbf{u} \end{bmatrix} [1 \quad \mathbf{u}^T] d\mathbf{u} \\ &= \int_{-\pi/2}^{\pi/2} \cos \psi \int_0^{2\pi} \tilde{R}_{\mathbf{u}}(\tau) \begin{bmatrix} 1 \\ \mathbf{u} \end{bmatrix} [1 \quad \mathbf{u}^T] d\phi d\psi \end{aligned} \quad (13)$$

where  $\phi$  and  $\psi$  represent azimuth and elevation, respectively.

If the noise is azimuthally independent, i.e., the functions  $\tilde{R}_{\mathbf{u}}(\tau)$  are identical for all directions with a given elevation, we can use the notation  $\tilde{R}_{\psi}(\tau)$ . Such an assumption, is generally

appropriate in azimuthally symmetric ocean when wind-generated noise is dominant, and is widely used, (see, for example, [18] and [21]). Equation (13) then becomes

$$\begin{aligned} R(\mathbf{0}, \tau) &= 2\pi \int_{-\pi/2}^{\pi/2} \tilde{R}_{\psi}(\tau) \cos \psi \\ & \cdot \begin{bmatrix} 1 & 0 & 0 & \sin \psi \\ 0 & (\cos^2 \psi)/2 & 0 & 0 \\ 0 & 0 & (\cos^2 \psi)/2 & 0 \\ \sin \psi & 0 & 0 & \sin^2 \psi \end{bmatrix} d\psi. \end{aligned} \quad (14)$$

The co-located cross-covariances, except that between pressure and the vertical velocity component, are zero at all lags. Therefore, a sensor consisting of a pressure component and two orthogonal horizontal velocity components, known as a DIFAR sensor and of interest as a multistatic active receiver [25], will have a diagonal-noise covariance matrix at all lags. In addition, the auto-covariances of the two horizontal velocity components are identical, and so the auto-covariance of any horizontal velocity component is the same. Since  $\tilde{R}_{\psi}(0) \geq 0$ , the pressure-sensor noise power is larger than any of the velocity-sensor noise powers. A sensor that measures one velocity component performs spatial filtering with a cosine response function, thus attenuating signals from many of the directions that contribute to the overall noise power. When the pressure-sensor noise power is greater than the velocity-sensor noise power, the performance advantages that vector-sensor systems possess over pressure-sensor systems are magnified [3].

If the noise field is also symmetric in elevation, i.e.,  $\tilde{R}_{\psi}(\tau) = \tilde{R}_{-\psi}(\tau)$  for all  $\tau$ , then the function  $f(\psi) = \tilde{R}_{\psi}(\tau) \cos \psi \sin \psi$  is anti-symmetric so that the cross-correlation between pressure and the vertical velocity component also becomes zero. Therefore, a complete four-component vector sensor would have diagonal-noise covariance at all lags.

When the noise is spherically isotropic, planewaves from all directions have the same autocorrelation function. Substituting  $\tilde{R}_{\mathbf{u}}(\tau) = \tilde{R}(\tau)$  in (13) and evaluating results in

$$R(\mathbf{0}, \tau) = 4\pi \tilde{R}(\tau) \begin{bmatrix} 1 & 0 \\ 0 & I_3/3 \end{bmatrix}. \quad (15)$$

Therefore, all auto-covariances have the same temporal structure (proportional to the auto-covariance of the individual planewaves used to construct the field), and the noise power at the pressure sensor's output is three times that in each velocity sensor's output.

The above assumptions can be relaxed so that the azimuthal independence, elevational symmetry, or spherical isotropy, hold for a particular value of  $\tau$  instead of all  $\tau$ . The results then hold for that particular lag value. In particular, for  $\tau = 0$ , we are merely making assumptions regarding the noise power  $\tilde{R}_{\mathbf{u}}(0)$  coming from each direction rather than the complete power spectral density (PSD), and the results apply to  $R(\mathbf{0}, \mathbf{0})$ , i.e., the covariance matrix of a single snapshot. We also note that, regardless of the spatial symmetry of  $\tilde{R}_{\mathbf{u}}(\tau)$  i) if there exists some value of  $\tau$ , say  $\tau_0$ , such that  $\tilde{R}_{\mathbf{u}}(\tau_0) = 0$  for all  $\mathbf{u}$ ,

then the snapshots of a vector sensor sampled at  $1/\tau_0$  would be uncorrelated and identically distributed; ii) if the PSD of each planewave is symmetric about the center frequency  $\omega_c$  then  $\tilde{R}_{\mathbf{u}}(\tau)$  is purely real for all  $\mathbf{u}$  and all  $\tau$  (see [26, p. 280]), and so every entry of  $R_{\mathbf{u}}(\mathbf{0}, \tau)$  is real for all  $\tau$ .

#### A. Between-Sensor Covariances

We now consider the cross-covariances between the outputs of two vector sensors separated by a vector displacement  $\mathbf{d}$ . To obtain expressions any less complex than (12) we must make the narrowband assumption that, for each direction  $\mathbf{u}$ ,  $\tilde{R}_{\mathbf{u}}(\tau + \mathbf{u}^T \mathbf{d}/c) \approx \tilde{R}_{\mathbf{u}}(\tau)$  for all  $\tau$ . This is exactly true when  $\mathbf{u}$  is orthogonal to the direction of separation and imposes the most stringent bandwidth constraint biggest constraint when  $\mathbf{d}$  and  $\mathbf{u}$  are parallel; it is essentially the standard narrowband array processing assumption. We can now write

$$R(\mathbf{d}, \tau) = \int_{\mathcal{U}} \tilde{R}_{\mathbf{u}}(\tau) e^{i\omega_c \mathbf{u}^T \mathbf{d}/c} \begin{bmatrix} 1 \\ \mathbf{u} \end{bmatrix} [1 \quad \mathbf{u}^T] d\mathbf{u}. \quad (16)$$

As before, suppose that  $\tilde{R}_{\mathbf{u}}(\tau)$  is azimuthally independent. Writing  $\mathbf{l} = \omega_c \mathbf{d}/c$ , and using the notation  $\bar{\mathbf{l}}$  and  $\bar{\mathbf{u}}$  for the projections onto the horizontal of  $\mathbf{l}$  and  $\mathbf{u}$ , respectively, equation (16) becomes

$$R(\mathbf{d}, \tau) = \int_{-\pi/2}^{\pi/2} \tilde{R}_{\psi}(\tau) e^{il_3 \sin \psi} \cdot \cos \psi \int_0^{2\pi} e^{i\bar{\mathbf{u}}^T \bar{\mathbf{l}}} \begin{bmatrix} 1 \\ \mathbf{u} \end{bmatrix} [1 \quad \mathbf{u}^T] d\phi d\psi \quad (17)$$

$$= 2\pi \int_{-\pi/2}^{\pi/2} T \tilde{R}_{\psi}(\tau) e^{il_3 \sin \psi} \cos \psi d\psi \quad (18)$$

where  $l_3$  is the vertical component of  $\mathbf{l}$  and  $T$  is a symmetric  $4 \times 4$  matrix  $T$  whose upper-diagonal entries are (see Appendix A)

$$T_{11} = J_0(|\bar{\mathbf{l}}| \cos \psi)$$

$$T_{1(m+1)} = iJ_1(|\bar{\mathbf{l}}| \cos \psi) \cos \psi \cos \gamma_m$$

$$T_{14} = J_0(|\bar{\mathbf{l}}| \cos \psi) \sin \psi$$

$$T_{23} = \left\{ \frac{J_0(|\bar{\mathbf{l}}| \cos \psi) - J_2(|\bar{\mathbf{l}}| \cos \psi)}{2} \cos \psi - \frac{J_1(|\bar{\mathbf{l}}| \cos \psi)}{|\bar{\mathbf{l}}|} \right\} \cos \psi \cos \gamma_1 \cos \gamma_2$$

$$T_{(m+1)4} = iJ_1(|\bar{\mathbf{l}}| \cos \psi) \cos \psi \sin \psi \cos \gamma_m$$

$$T_{(m+1)(m+1)} = \frac{J_0(|\bar{\mathbf{l}}| \cos \psi) - J_2(|\bar{\mathbf{l}}| \cos \psi)}{2} \cos^2 \psi \cos^2 \gamma_m + \frac{J_1(|\bar{\mathbf{l}}| \cos \psi)}{|\bar{\mathbf{l}}|} \cos \psi \sin^2 \gamma_m$$

$$T_{44} = J_0(|\bar{\mathbf{l}}| \cos \psi) \sin^2 \psi \quad (19)$$

for  $m = 1, 2$ , where  $J_k(\cdot)$  is the  $k$ th-order Bessel function of the first kind, and  $\gamma_m$  is the angle between the horizontal com-

ponent of displacement and the  $m$ th axis. The actual correlation structure will thus be fairly complex, however, we can make the following observations: 1)  $T_{23}$  is proportional to  $\cos \gamma_1 \cos \gamma_2$ . Thus, the magnitude of the correlation between the horizontal-velocity sensors is a maximum when the horizontal component of displacement makes a  $45^\circ$  angle with both axes. When this is the case,  $|T_{12}| = |T_{13}|$  and  $|T_{24}| = |T_{34}|$ , and so the magnitude of the covariance between pressure and both horizontal velocity sensors is the same, as is that between vertical velocity and both horizontal velocity sensors; 2)  $T_{1(m+1)}$  and  $T_{(m+1)4}$  are proportional to  $\cos \gamma_m$ , for  $m = 1, 2$ , so the correlation between a pressure sensor or vertical velocity sensor and a horizontal velocity sensor is zero for all  $\tau$  if the displacement  $\mathbf{d}$  is orthogonal to the horizontal velocity sensor's axis; and 3) Again, since  $T_{23}$  is proportional to  $\cos \gamma_1 \cos \gamma_2$ , the correlation between orthogonally-oriented horizontal velocity sensors is zero if  $\mathbf{d}$  is orthogonal to either sensor's axis. In particular, when  $\mathbf{d}$  is vertical, only the correlations between like sensors and between pressure and vertical velocity are nonzero. In fact

$$R(\mathbf{d}, \tau) = \int_{-\pi/2}^{\pi/2} \tilde{R}_{\psi}(\tau) e^{il_3 \sin \psi} \cos \psi \cdot \int_0^{2\pi} \begin{bmatrix} 1 \\ \mathbf{u} \end{bmatrix} [1 \quad \mathbf{u}^T] d\phi d\psi \quad (20)$$

$$= 2\pi \int_{-\pi/2}^{\pi/2} \tilde{R}_{\psi}(\tau) e^{il_3 \sin \psi} \cos \psi \cdot \begin{bmatrix} 1 & 0 & 0 & \sin \psi \\ 0 & (\cos^2 \psi)/2 & 0 & 0 \\ 0 & 0 & (\cos^2 \psi)/2 & 0 \\ \sin \psi & 0 & 0 & \sin^2 \psi \end{bmatrix} d\psi \quad (21)$$

which has a similar structure to (14), the covariance matrix of a single vector sensor. It follows that the cross-correlation between any two parallel horizontal velocity sensors is independent of their common orientation. We may also observe that the cross-covariances between like sensors satisfy the relationship

$$\text{tr} R(\mathbf{d}, \tau) = 2R(\mathbf{d}, \tau)_{11}. \quad (22)$$

We now include the condition of elevational symmetry, and again consider an arbitrary displacement  $\mathbf{d}$ . In this case,  $\tilde{R}_{\psi}(\tau) \cos(l_3 \sin \psi) \cos \psi$  is a symmetric function of  $\psi$ , while  $\tilde{R}_{\psi}(\tau) \sin(l_3 \sin \psi) \cos \psi$  is anti-symmetric. In addition, all the entries of  $T$  are either symmetric or anti-symmetric functions of  $\psi$ . It can thus be shown that the upper-diagonal entries of the symmetric matrix  $R(\mathbf{d}, \tau)$  can be written

$$R(\mathbf{d}, \tau)_{mn} = 4\pi \int_0^{\pi/2} T_{mn} \tilde{R}_{\psi}(\tau) f_{mn}(l_3 \sin \psi) \cos \psi d\psi \quad (23)$$

for  $m \leq n = 1, \dots, 4$ , where  $f_{mn}(\cdot) = i \sin(\cdot)$  for  $(m, n) = (1, 4), (2, 4),$  and  $(3, 4)$ , and  $f_{mn}(\cdot) = \cos(\cdot)$  otherwise. Furthermore, if  $\tilde{R}_{\psi}(\tau)$  is real, e.g.,  $\tau = 0$  or the PSDs are symmetric about the center frequency, the  $(1, 2), (1, 3),$  and  $(1, 4),$

entries of  $R(\mathbf{d}, \tau)$  are purely imaginary and the remainder are purely real, i.e., correlations between pressure and velocity sensors are imaginary, but all other correlations are real.

Finally, we consider the case of spherically-isotropic noise. Equation (16) now becomes

$$R(\mathbf{d}, \tau) = \tilde{R}(\tau) \int_{\mathcal{U}} e^{i\mathbf{u}^T \boldsymbol{\tau}} \begin{bmatrix} 1 \\ \mathbf{u} \end{bmatrix} [1 \quad \mathbf{u}^T] d\mathbf{u} = 4\pi \tilde{R}(\tau) M \quad (24)$$

where  $M$  is a  $4 \times 4$  matrix with entries (see Appendix B)

$$\begin{aligned} M_{11} &= j_0(|\boldsymbol{\tau}|) \\ M_{1(m+1)} &= M_{(m+1)1} = i j_1(|\boldsymbol{\tau}|) \cos \gamma_m \\ M_{(m+1)(n+1)} &= -j_2(|\boldsymbol{\tau}|) \cos \gamma_m \cos \gamma_n \quad m \neq n \\ M_{(m+1)(m+1)} &= \frac{j_1(|\boldsymbol{\tau}|)}{|\boldsymbol{\tau}|} - j_2(|\boldsymbol{\tau}|) \cos^2 \gamma_m \end{aligned} \quad (25)$$

for  $m, n = 1, 2, 3$  where  $j_k(\cdot)$  is the  $k$ th-order spherical Bessel function. Therefore, all correlations have the same temporal structure. In general, none of the entries of  $R(\mathbf{d}, \tau)$  are zero. Even when the sensor separation is half a wavelength, the only correlation that is always zero is that between the pressure sensors. As above, if  $\tilde{R}(\tau)$  is real, the correlation between pressure and each velocity component is always imaginary, while the other correlations are purely real.

Fig. 1 shows the correlations encapsulated by the matrix  $M$ , as a function of the separation distance. The solid curve is  $M_{11}$ , the pressure–pressure correlation, which is independent of the direction of displacement. The dashed curve is the pressure–velocity correlation  $M_{(m+1)1}$  when  $\gamma_m = 0$ , i.e., the direction of separation  $\mathbf{d}$  lies along the  $m$ th velocity sensor’s axis. This is the maximum value of  $M_{(m+1)1}$ , the minimum value being zero when  $\mathbf{d}$  is orthogonal to the sensor’s axis. The dash-dotted curve is the maximum value of the correlation between orthogonal velocity components, i.e.,  $M_{(m+1)(n+1)}$  for  $m \neq n$ , which is attained when the separation direction lies in the plane of the  $m$ th and  $n$ th sensors’ axes and  $45^\circ$  between them. The minimum value is zero when  $\mathbf{d}$  is orthogonal to one of the axes. The final two curves show the correlation between similarly-oriented velocity sensors  $M_{(m+1)(m+1)}$  for the cases when their axis is orthogonal to  $\mathbf{d}$  (large dots), and parallel to  $\mathbf{d}$  (small dots). In general,  $M_{(m+1)(m+1)}$  will lie between these two curves.

Notice that for a separation of around 0.95 wavelengths (and multiples thereof), all curves, except  $j_1(|\boldsymbol{\tau}|)$  are close to zero. Thus, whatever the direction of separation the pressure–pressure correlation and all velocity–velocity correlations are nearly zero, only the pressure–velocity correlations may differ significantly from zero. Furthermore, the latter correlations are simultaneously minimized by choosing  $\mathbf{d}$  such that the  $\gamma_m$  are all equal, e.g.,  $\mathbf{d} \propto [1, 1, 1]^T / \sqrt{3}$ . In that case, each  $M_{(m+1)1}$  is  $1/\sqrt{3}$  times its maximum shown in the figure, which is about  $-0.1$  when the separation is 0.95 wavelengths. This arrangement, therefore, minimizes the largest cross-covariance. To be

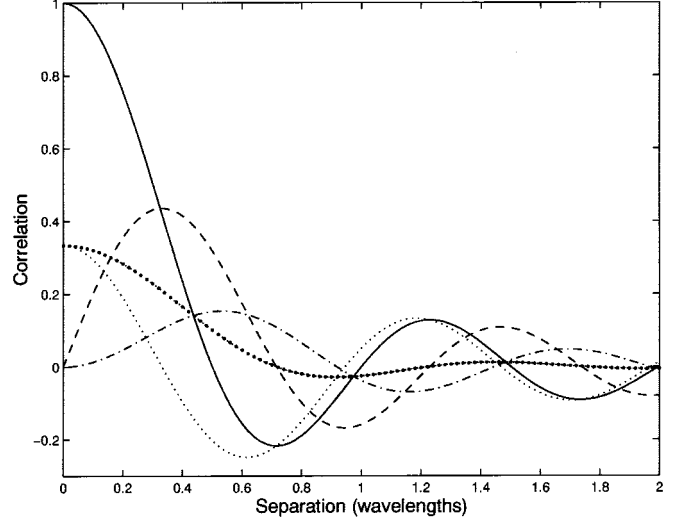


Fig. 1. Cross-correlations in spatially-isotropic noise as function of sensor separation. Solid is  $j_0(|\boldsymbol{\tau}|)$ , dashed is  $j_1(|\boldsymbol{\tau}|)$ , dash-dotted is  $j_2(|\boldsymbol{\tau}|)/2$ , large dotted is  $j_1(|\boldsymbol{\tau}|)/|\boldsymbol{\tau}|$ , and small dotted is  $j_1(|\boldsymbol{\tau}|)/|\boldsymbol{\tau}| - j_2(|\boldsymbol{\tau}|)$ .

specific, when  $\mathbf{d} = 0.95[1, 1, 1]^T / \sqrt{3}$  wavelengths, the cross-covariance matrix is

$$R(\mathbf{d}, \tau) = 4\pi \tilde{R}(\tau) \begin{bmatrix} -0.05 & -0.1i & -0.1i & -0.1i \\ -0.1i & -0.02 & 0.01 & 0.01 \\ -0.1i & 0.01 & -0.02 & 0.01 \\ -0.1i & 0.01 & 0.01 & -0.02 \end{bmatrix}. \quad (26)$$

Thus, a uniform linear array (ULA) of identically oriented vector sensors, whose common orientation is such that the array’s axis forms the same angle ( $54.74^\circ$ ) to each of the three velocity sensor axes, and whose inter-sensor spacing is 0.95 wavelengths, would have an approximately diagonal covariance matrix. No off-diagonal element would be larger than about 10% of the pressure sensor auto-covariance, which is  $4\pi \tilde{R}(\tau)$  [see equation (15)]. Note that as shown in [3], spacings of more than half a wavelength do not lead to ambiguities with a vector sensor ULA.

As a final example, consider the commonly used vertical linear ULA configuration with half wavelength spacing and suppose the velocity sensors are aligned with the coordinate axes. In this case the within sensor covariance is given by (15) and the covariance between adjacent vector sensors is

$$R(\mathbf{d}, \tau) = 4\pi \tilde{R}(\tau) \begin{bmatrix} 0 & 0 & 0 & 0.32i \\ 0 & 0.10 & 0 & 0 \\ 0 & 0 & 0.10 & 0 \\ 0.32i & 0 & 0 & -0.20 \end{bmatrix}. \quad (27)$$

A similar pressure-sensor array would have a diagonal-noise covariance.

#### IV. PERFORMANCE OF A LINEAR ARRAY

In this section, we quantitatively examine the effect of isotropic and anisotropic-noise fields on the localization accuracy and beamforming performance of an AVS array.

The Cramér–Rao bound is a lower bound on the variance of all unbiased estimates of a parameter and is asymptotically achieved by the maximum-likelihood estimator (under very mild regularity conditions), see e.g., [27]. It is therefore a very useful measure of the performance achievable with a given array. Consider an  $m$  element AVS array illuminated by  $n$  narrowband far-field sources, with directions of arrival,  $\boldsymbol{\theta} = [\boldsymbol{\theta}_1^T, \dots, \boldsymbol{\theta}_n^T]^T$ , where each  $\boldsymbol{\theta}_i = [\phi_i, \psi_i]$  contains the azimuth and elevation, respectively of the  $i$ th source. The array output is a  $4m \times 1$  vector  $\mathbf{y}(t)$  given by [2], [3]

$$\mathbf{y}(t) = A(\boldsymbol{\theta})\mathbf{p}(t) + \mathbf{e}(t) \quad (28)$$

where

$$\begin{aligned} A(\boldsymbol{\theta}) &= [\mathbf{a}(\boldsymbol{\theta}_1), \dots, \mathbf{a}(\boldsymbol{\theta}_n)]; \\ \mathbf{p}(t) &\text{ contains source signals;} \\ \mathbf{e}(t) &\text{ noise.} \end{aligned}$$

The steering vector of the  $i$ th source is

$$\mathbf{a}(\boldsymbol{\theta}_i) = \begin{bmatrix} e^{i2\pi\mathbf{r}_1^T\mathbf{u}_i} \\ \vdots \\ e^{i2\pi\mathbf{r}_m^T\mathbf{u}_i} \end{bmatrix} \otimes \begin{bmatrix} 1 \\ \mathbf{u}_i \end{bmatrix} \quad (29)$$

where  $\mathbf{u}_i$  is the (unit-length) bearing vector in the direction of the  $i$ th source, and  $\mathbf{r}_i$  are the sensor locations (in wavelengths) relative to the phase center of the array.

Assume that  $\mathbf{s}(t)$  and  $\tilde{\mathbf{e}}(t)$  are independent and identically distributed (i.i.d), zero-mean, complex Gaussian processes, that are uncorrelated with other, and have covariance matrices

$$E\{\mathbf{p}(t)\mathbf{p}^H(t)\} = P \quad (30)$$

$$E\{\mathbf{e}(t)\mathbf{e}^H(t)\} = \sigma^2\Sigma \quad (31)$$

where  $\Sigma$  is a known positive definite Hermitian matrix, but  $P$  and  $\sigma^2$  are unknown. Then, the output  $\mathbf{y}(t)$  is an i.i.d zero-mean complex Gaussian process with covariance  $R = APA^H + \sigma^2\Sigma$ , where we have suppressed the dependence of  $A$  on  $\boldsymbol{\theta}$  for notational convenience.

Since  $\Sigma$  is positive definite and Hermitian, there exists a positive definite Hermitian matrix  $\Sigma^{1/2}$  such that  $\Sigma = \Sigma^{1/2}\Sigma^{1/2}$ . Let

$$\tilde{\mathbf{y}}(t) = \Sigma^{-1/2}\mathbf{y}(t) = \tilde{A}\mathbf{s}(t) + \tilde{\mathbf{e}}(t) \quad (32)$$

where  $\tilde{A} = \Sigma^{-1/2}A$  and  $\tilde{\mathbf{e}}(t) = \Sigma^{-1/2}\mathbf{e}(t)$ . Then,  $\tilde{\mathbf{y}}(t)$  is a zero-mean, Gaussian process with covariance  $\tilde{R} = \tilde{A}P\tilde{A}^H + \sigma^2I$ . The transformation (32) does not alter the CRB because it is a known invertible linear transformation and  $\mathbf{y}(t)$  is Gaussian. This may be shown by using Bangs' formula (see e.g., [28, p. 525]) to calculate the entries of the Fisher information matrix (FIM), using both  $\tilde{R}$  and  $R$ . The results are identical.

In [2] an expression was given for the CRB on the direction parameters  $\boldsymbol{\theta}$  for models of the form (32). This expression requires inversion of a matrix whose order is equal to the number of elements in  $\boldsymbol{\theta}$  rather than the full FIM. Using [2, Theorem

3.1] and (32) we can show that the CRB on azimuth and elevation for a single source is the  $2 \times 2$  matrix

$$\begin{aligned} \text{CRB}(\boldsymbol{\theta}) &= \frac{1}{2N\rho} \left( 1 + \frac{1}{\mathbf{a}^H\Sigma^{-1}\mathbf{a}\rho} \right) \\ &\cdot \left[ \Re \left\{ D^H\Sigma^{-1} \left( I - \frac{\mathbf{a}\mathbf{a}^H\Sigma^{-1}}{\mathbf{a}^H\Sigma^{-1}\mathbf{a}} \right) D \right\} \right]^{-1} \end{aligned} \quad (33)$$

where  $\rho = P/\sigma^2$  is the SNR,  $N$  is the number of snapshots, and

$$D = [\partial\mathbf{a}/\partial\phi, \partial\mathbf{a}/\partial\psi] \quad (34)$$

where  $\phi$  and  $\psi$  are the azimuth and elevation of the source, respectively. Since there are two source location parameters, a useful overall measure of optimal localization accuracy is given by the following bound on the mean-square angular error (see [2] and [29])

$$\text{MSAE}_B = \cos^2\psi \text{CRB}(\phi) + \text{CRB}(\psi). \quad (35)$$

Expanding (33) by substituting the expression for  $\mathbf{a}$  from (29) does not lead to particularly insightful expressions (except in the case  $\Sigma = I$ , i.e., white noise, see [3], [4]). Therefore, we will examine the CRB and  $\text{MSAE}_B$  for some specific numerical examples.

We consider two anisotropic-noise fields in which the spatial power density of the noise power is proportional to the radius of a prolate and an oblate spheroid, respectively. A prolate spheroid is obtained by revolving an ellipse, which lies in the  $x, z$ -plane with its major axis in the  $x$ -direction, about the  $z$ -axis. The result is a sphere with flattened poles. An oblate spheroid is obtained by revolving an ellipse, which lies in the  $x, z$ -plane with its major axis in the  $z$ -direction, about the  $z$ -axis. The result is an (American) football shape. Therefore, more noise comes from directions near the horizontal than near the vertical in the prolate spheroid field, while the reverse is true in the oblate spheroid field. Note that both noise fields are azimuthally independent and elevationally symmetric. Pressure-sensor correlations in a prolate-noise field were examined in [21].

For the prolate spheroid, we have

$$\tilde{R}_\psi(0) \propto \sqrt{\frac{1 - \epsilon^2}{1 - \epsilon^2 \cos^2 \psi}} \quad (36)$$

and for the oblate spheroid

$$\tilde{R}_\psi(0) \propto \sqrt{\frac{1 - \epsilon^2}{1 - \epsilon^2 \sin^2 \psi}} \quad (37)$$

where  $\epsilon$  is the eccentricity of the ellipse that is used to form the solid of revolution. It is given by  $\epsilon = \sqrt{a^2 - b^2}/a$ , where  $a$  and  $b$  are the lengths of the semi-major and semi-minor axes, respectively. When  $\epsilon = 0$  both shapes are spheres, i.e.,  $\epsilon = 0$  corresponds to spherically-isotropic noise. As  $\epsilon \rightarrow 1$ , the prolate-noise field becomes a cylindrically symmetric (two-dimensional)-noise field, in which noise only arrives from the horizontal and is evenly distributed in azimuth. For the oblate field,

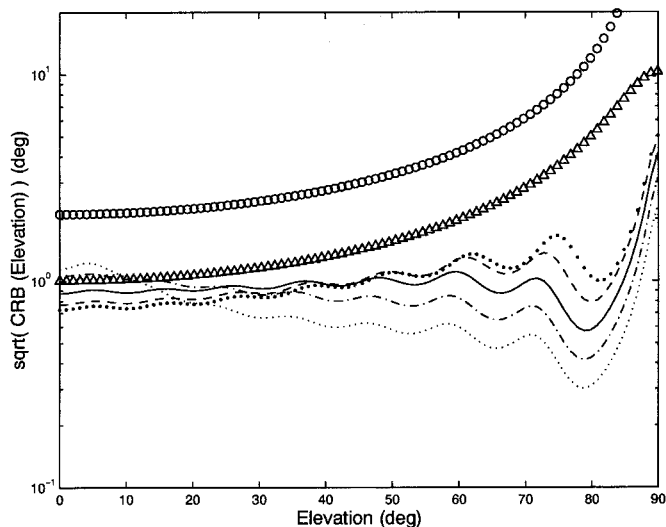


Fig. 2. Single-snapshot  $\text{CRB}(\psi)$  for AVS array in spherically-isotropic noise (solid), anisotropic noise with eccentricity  $-15$  dB (large dots),  $-6$  dB (dash),  $6$  dB (dash-dot),  $15$  dB (small dots), and white noise ( $\Delta$ ). Also shown is CRB for pressure-sensor array in spherically-isotropic noise ( $o$ ).

noise comes from just two directions, the zenith and the nadir, as  $\epsilon \rightarrow 1$ . In the following, we express the eccentricity as the ratio of the power density in the horizontal direction to that in the vertical, i.e.,  $\rho_\epsilon = \tilde{R}_0(0)/\tilde{R}_{\pi/2}(0)$ . It follows that, when expressed in dB,  $\rho_\epsilon$  is positive for the prolate-noise field and negative for the oblate, while  $0$  dB corresponds to spherically-isotropic noise.

In these examples, we consider half-wavelength spaced vertical ULAs of pressure sensors and vector sensors (the latter with their velocity sensing elements aligned with the coordinate axes). We suppose there are eight sensors in each array and a signal-to-noise ratio (SNR) of  $0$  dB, defined as the signal power to the noise power at each pressure sensing element. With  $\rho = P/\sigma^2$ , as above, this implies that  $\Sigma$  is normalized such that the entries  $\Sigma_{(4k+1)(4k+1)}$ , for  $k = 0, 1, \dots$  are all unity. To make a fair comparison between internal sensor noise (i.e., white noise) and ambient noise for the AVS array, we define the SNR for the former slightly differently. We compare an AVS array in white noise with an AVS array in ambient noise when they have the same total vector sensor-noise power defined as  $\text{tr}\{R(\mathbf{0}, \mathbf{0})\}$ . It follows from (22) that when the noise is azimuthally independent  $\text{tr}\{R(\mathbf{0}, \mathbf{0})\} = 2\sigma^2$ . Since  $\text{tr}\{R(\mathbf{0}, \mathbf{0})\} = 4\sigma^2$  for white noise, we define the SNR as  $\rho/2$ . The entries of the noise covariance  $\Sigma$  are obtained from (23), with  $l_3 = \pi k$  for  $k = 0, \dots, 7$ , and using (36) and (37) for the prolate and oblate fields respectively.

Fig. 2 shows the CRB on elevation for the AVS array in ambient-isotropic, prolate and oblate-noise fields, and assuming white noise. The CRB for the pressure-sensor array in ambient-isotropic noise, when its covariance matrix is spatially white, is also shown. The bound is independent of the azimuth due to the symmetry of the problem. The AVS array's performance is considerably better at all angles than that of the pressure-sensor array, due to the greater number of measurements and the directionality of its sensors (see [3] for a comparison of the two arrays in white noise). It also remains finite, whatever, the noise

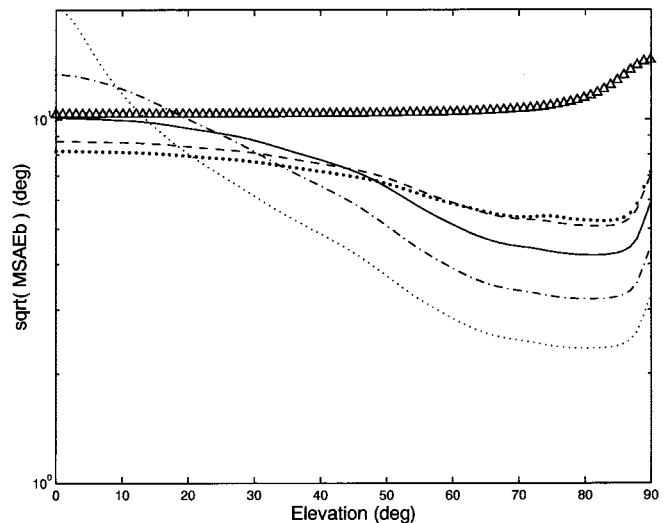


Fig. 3. Single-snapshot  $\text{MSAE}_B$  for AVS array in spherically-isotropic noise (solid), anisotropic noise with eccentricity  $-15$  dB (large dot),  $-6$  dB (dash),  $6$  dB (dash-dot),  $15$  dB (small dot), and white noise ( $\Delta$ ).

field, as the source tends to endfire. Naturally, near endfire a prolate-noise distribution results in a lower bound than an oblate, since there is less noise coming from directions near the signal. The reverse is the case near broadside. More surprising, is that fact that, for all ambient-noise fields in this example, the CRB is lower than in the white noise case, for most directions. The latter only improves upon the two prolate cases within  $10^\circ$  of the horizontal, and is nowhere better than the isotropic or oblate. Another interesting feature is that the curves corresponding to ambient fields are undulating while that for white noise is smooth. In fact, they exhibit a particularly significant dip near  $80^\circ$ , with the result that this is the best direction even for the isotropic case. A somewhat surprising result, given that linear arrays tend to perform best for sources near broadside and worst for sources near endfire, because of the difference in effective visible aperture (see discussions in [30], [3], [4]). In fact the performance only noticeable deteriorates within a few degrees of endfire.

When the noise is uncorrelated, it evenly fills the measurement space. The CRB is then just dependent on the visible aperture. When correlated, however, the noise is more concentrated in some subspaces than others. If the correlation causes the noise in the signal subspace to be smaller than it would be in white noise, then it will be possible to more accurately estimate the signal's direction. Clearly, the interaction between the AVS array's steering vector and the noise correlation is such that less noise is in the subspace corresponding to directions near endfire than near broadside. In addition, for the isotropic and oblate fields, the correlation structure causes less noise to be placed in the subspaces corresponding to all angles, than is the case with white noise.

Fig. 3 shows the  $\text{MSAE}_B$ . It is somewhat larger indicating that the majority of error is due to uncertainty in the azimuth (the pressure-sensor array is unable to determine azimuth at all). This time the curves are much smoother, but it is clear that the overall performance, for all ambient models, improves as the source moves toward endfire. In fact all ambient curves attain

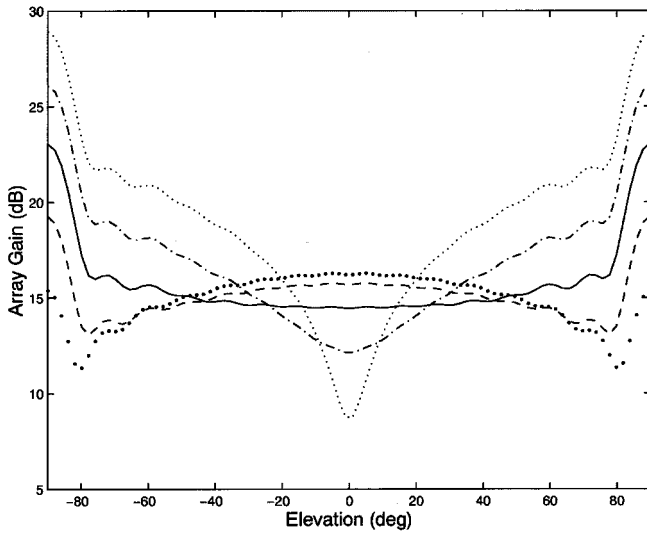


Fig. 4. Array gain for AVS array in spherical-isotropic noise (solid), and anisotropic noise with eccentricity  $-15$  dB (large dots),  $-6$  dB (dash),  $6$  dB (dash-dot), and  $15$  dB (small dots).

their best performance for source coming from  $85^\circ$  and their endfire performance is better than their broadside. This contrasts strongly with the  $MSAE_B$  for the white-noise situation, where the performance deteriorates consistently as the source approaches endfire. It is also interesting that in the isotropic and oblate fields the  $MSAE_B$  lies within a range of 5 or 6 degrees (note the logarithmic scale), but varies much more dramatically in the prolate fields.

In conventional beamforming, a fixed linear combination of the outputs is formed to maximize the gain to signals from a particular direction, while minimizing the noise or the gain presented to signals from other directions. Using the pre-whitened data  $\tilde{\mathbf{y}}(t)$ , the beamformer output power is

$$E\tilde{z}^2 = E|\mathbf{w}^H \tilde{\mathbf{y}}(t)|^2 = P\mathbf{w}^H \Sigma^{-1/2} \mathbf{a}\mathbf{a}^H \Sigma^{-1/2} + \sigma^2 |\mathbf{w}|^2 \quad (38)$$

when there is a single source, where  $\mathbf{w}$  is the beamforming weight vector. To maximize the gain to a signal with steering vector  $\mathbf{a}_s$ , the weight vector should be chosen such that it is proportional to the transformed steering vector  $\tilde{\mathbf{a}}_s$ , i.e.,  $\mathbf{w} = \Sigma^{-1/2} \mathbf{a}_s / |\Sigma^{-1/2} \mathbf{a}_s|$ . The array gain is the ratio of signal gain to noise gain in the output of the beamformer, when the beamformer is matched to the signal, i.e.,  $\mathbf{a}_s = \mathbf{a}$ . It follows from (38) that the array gain is  $|\mathbf{a} \Sigma^{-1} \mathbf{a}|$ . If the noise is spatially white, the array gain is independent of the source direction (15 dB for the present scenario), however this is not the case if the noise is correlated.

Fig. 4 shows the array gain of the AVS array for isotropic, prolate, and oblate-noise fields. As the noise field becomes more prolate, the gain near endfire improves even further, but near broadside it declines. Conversely, as the noise field becomes more oblate, the gain to a signal arriving from near the horizontal improves while that to a signal near endfire declines. Obviously, when much of the noise comes from directions similar to the that of signal, we may expect the beamformer's performance to become worse. In spherical-isotropic noise, the array gain is very similar to the white noise gain between  $-45^\circ$  and

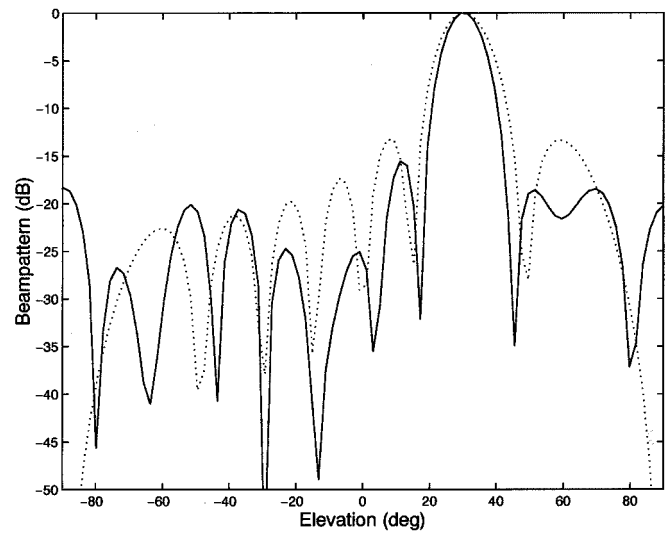


Fig. 5. Beampattern for AVS array steered to  $30^\circ$  elevation in spherical-isotropic noise (solid) and white noise (small dots).

$45^\circ$  and is significantly greater nearer endfire. Except for the most eccentric oblate field, the endfire array gain is greater than that near broadside. To explain this, we note that, unlike the pressure-sensor array, the AVS array is easily able to discriminate between endfire directions. Therefore, when the beamformer is matched to a signal near endfire, the noise at the output is mostly that propagating from a small range of angles close to that endfire direction. Furthermore, since it is vertical, the AVS array, can discriminate between signals separated in elevation much better than it can signals separated in azimuth. So, ignoring the much weaker azimuthal filtering capabilities, and assuming that signals more than  $15^\circ$  elevation away from the steering direction are mostly suppressed, a beamformer matched to  $85^\circ$  would have a noise output power approximately proportional to

$$\int_0^{2\pi} \int_{70^\circ}^{90^\circ} \tilde{R}_{\psi}(0) d\psi d\phi. \quad (39)$$

However, when matched to broadside, the noise-output power would be approximately proportional to

$$\int_0^{2\pi} \int_{-15^\circ}^{15^\circ} \tilde{R}_{\psi}(0) d\psi d\phi. \quad (40)$$

Now, the noise, even if isotropic, is not evenly distributed in elevation, that is the total noise power arising from all directions in a narrow range of elevations  $\psi + \Delta\psi$  is much larger if  $\psi$  is near broadside than near endfire. It follows that (40) may be considerably larger than (39), which explains the observed behavior.

The beampattern is the gain presented to signals from all directions, when the array is steered to a particular fixed direction and is given by  $(\mathbf{a}_s \Sigma^{-1} \mathbf{a})^2$ . Fig. 5 shows the AVS array's normalized beampattern, steered to  $\psi_s = 30^\circ$ , as a function of elevation, in white and isotropic noise. The beampattern will also vary with azimuth for the AVS array (but not the pressure-sensor array). We show the figure for the case where the azimuth of the signal and the steering direction are identical. In isotropic noise the beampattern has a narrower mainlobe and lower sidelobes

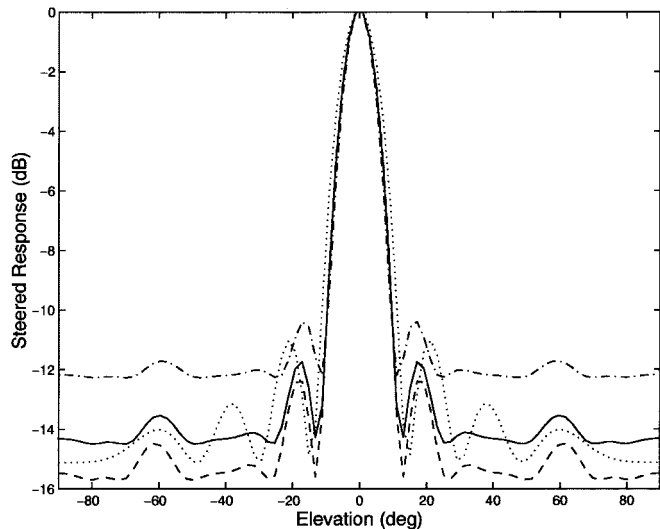


Fig. 6. Steered response of AVS array to a signal at  $0^\circ$  elevation in spherically-isotropic noise (solid), anisotropic noise with eccentricity  $-6$  dB (dash) and  $6$  dB (dash-dot), and white noise (small dots).

than in white noise. However, whereas the white-noise beamformer happens to completely null signal from either endfire for this steering direction, it is no longer the case in isotropic noise. There are a couple more interesting features in the isotropic beampattern: a very deep null at  $-\psi_s$  and a dip in the sidelobe level at  $2\psi_s$ . Furthermore, instead of decreasing uniformly toward endfire, the height of the sidelobes is actually smallest between  $0^\circ$  and  $-20^\circ$ . They then increase again further away from the steering direction. This one example suggests that the nature of beampatterns is generally much more complicated in ambient noise, even if isotropic, than in white noise.

A conventional beamformer can also be used for direction finding by searching for maxima in the steered response. The steered response is the output power ( $\mathbf{w}^H R \mathbf{w}$ ) of the beamformer for a fixed scenario, as the direction-of-look  $\mathbf{a}_s$  is changed. In practice  $R$  must be estimated from the data, Figs. 6 and 7 show the steered response when there is a single source located at broadside and  $60^\circ$  elevation, respectively. White, isotropic, prolate, and oblate-noise cases are illustrated. Features of the steered response can be used to make inferences concerning the direction estimate. The mainlobe width illustrates the ability resolve closely spaced sources; the narrow width, the better the resolution. It is essentially the same for all ambient-noise fields, however, in white noise it is somewhat larger, especially for the source near endfire. The greater the curvature at the peak of the response the smaller the asymptotic variance. Again, all three ambient-noise cases have a similar curvature, which is larger than the white noise case, especially near endfire. All the scenarios result in an asymptotically unbiased estimate because the maximum of each steered response coincides with the true source location. Finally, a higher sidelobe level corresponds to a higher probability of a wide-angle or “ambiguity” error in the direction estimate. For the broadside source, the white noise sidelobes are higher than the isotropic and oblate. For the  $60^\circ$  source, all three ambient fields result in a large sidelobe far from the mainbeam that is

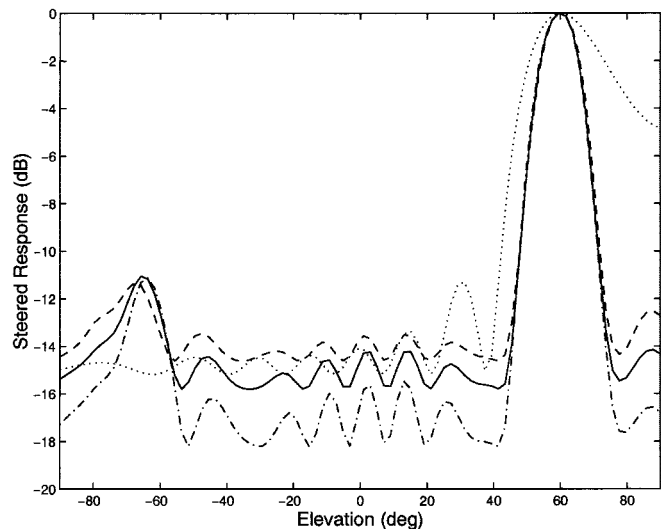


Fig. 7. Steered response of AVS array to a signal at  $60^\circ$  elevation in spherically isotropic noise (solid), anisotropic noise with eccentricity  $-6$  dB (dash) and  $6$  dB (dash-dot), and white noise (small dots).

about the same height as the largest sidelobe of white-noise beamformer.

## V. CONCLUSION

We derived closed-form and integral expressions for the auto and cross-covariances between the components of a single acoustic vector sensor, and for the cross-covariances between the components of two spatially separated vector sensors, in ambient-noise fields. We considered isotropic and anisotropic-noise fields with various assumptions on their spatial symmetry. We showed that, even in spherically-isotropic noise, no vector-sensor array can have a diagonal-noise co-variance, although a ULA with a certain separation and sensor orientation was found that minimized the maximum off-diagonal covariance. Using the results, we examined the effect of ambient noise on the performance of an AVS array through the CRB and a conventional beamformer. We showed that the direction estimation and beamforming capabilities can be substantially improved over the case in which the noise is spatially white. Furthermore, while an array in white noise will perform best when sources are near broadside, we showed that the CRB and array gain can be significantly better for sources close to endfire in ambient-noise fields. Detailed intuitive explanations for these observed phenomena were given (see Section IV).

## APPENDIX A

In this appendix we show that the entries of  $T$  are given by (19). The matrix  $T$  is

$$T = \frac{1}{2\pi} \int_0^{2\pi} e^{i\bar{\mathbf{u}}^T \bar{\mathbf{l}}} \begin{bmatrix} 1 \\ \mathbf{u} \end{bmatrix} [1 \quad \mathbf{u}] d\phi. \quad (41)$$

Letting  $\gamma$  be the angle between  $\bar{\mathbf{u}}$  and  $\bar{\mathbf{l}}$  and noting that  $|\bar{\mathbf{u}}| = \cos \psi$ , the (1, 1) entry can be written as

$$T_{11} = \frac{1}{2\pi} \int_0^{2\pi} e^{i|\bar{\mathbf{l}}| \cos \psi \cos \gamma} d\gamma = J_0(|\bar{\mathbf{l}}| \cos \psi). \quad (42)$$

Now

$$T_{1(m+1)} = \frac{1}{2\pi} \int_0^{2\pi} -i \frac{\partial}{\partial l_m} e^{i\bar{\mathbf{u}}^T \bar{\mathbf{l}}} d\phi = -i \frac{\partial}{\partial l_m} T_{11} \quad (43)$$

for  $m = 1, 2$ , where  $l_m$  is the  $m$ th entry of  $\bar{\mathbf{l}}$  (and also of  $\mathbf{l}$ ). The interchange of integration and differentiation is valid because  $e^{i\bar{\mathbf{u}}^T \bar{\mathbf{l}}}$  is continuous and the region of integration  $\phi \in [0, 2\pi]$  is compact. Similarly

$$T_{(m+1)(n+1)} = -\frac{\partial^2}{\partial l_m \partial l_n} T_{11} \quad (44)$$

for  $m, n = 1, 2$ . We shall make use of the following recurrence relations between Bessel functions and their derivatives (see [31, p. 357])

$$J_0^{(1)}(x) = -J_1(x) \quad (45)$$

$$J_0^{(2)}(x) = (J_2(x) - J_0(x))/2 \quad (46)$$

where superscript  $(n)$  indicates the  $n$ th derivative with respect to  $x$ . Using (42), (43), and (45), we have

$$\begin{aligned} T_{1(m+1)} &= -i \frac{l_m}{|\bar{\mathbf{l}}|} \cos \psi J_0^{(1)}(|\bar{\mathbf{l}}| \cos \psi) \\ &= i J_1(|\bar{\mathbf{l}}| \cos \psi) \cos \psi \cos \gamma_m. \end{aligned} \quad (47)$$

From (44)

$$\begin{aligned} T_{23} &= -l_1 \cos \psi \frac{\partial}{\partial l_2} \frac{J_0^{(1)}(|\bar{\mathbf{l}}| \cos \psi)}{|\bar{\mathbf{l}}|} \\ &= -\frac{l_1}{|\bar{\mathbf{l}}|^2} \cos \psi \left\{ l_2 \cos \psi J_0^{(2)}(|\bar{\mathbf{l}}| \cos \psi) \right. \\ &\quad \left. - \frac{l_2}{|\bar{\mathbf{l}}|} J_0^{(1)}(|\bar{\mathbf{l}}| \cos \psi) \right\} \\ &= \left\{ \frac{J_0(|\bar{\mathbf{l}}| \cos \psi) - J_2(|\bar{\mathbf{l}}| \cos \psi)}{2} \cos \psi \right. \\ &\quad \left. - \frac{J_1(|\bar{\mathbf{l}}| \cos \psi)}{|\bar{\mathbf{l}}|} \right\} \cos \psi \cos \gamma_1 \cos \gamma_2 \quad (48) \end{aligned}$$

where we have used (45) and (46) to obtain the last equality. Again, using (44)

$$\begin{aligned} T_{(m+1)(m+1)} &= -\frac{\partial}{\partial l_m} \frac{l_m}{|\bar{\mathbf{l}}|} \cos \psi J_0^{(1)}(|\bar{\mathbf{l}}| \cos \psi) \\ &= -\left\{ J_0^{(1)}(|\bar{\mathbf{l}}| \cos \psi) \left( \frac{|\bar{\mathbf{l}}|}{|\bar{\mathbf{l}}|^2} - \frac{l_m^2}{|\bar{\mathbf{l}}|^3} \right) \right. \\ &\quad \left. + \frac{l_m^2}{|\bar{\mathbf{l}}|^2} \cos \psi J_0^{(2)}(|\bar{\mathbf{l}}| \cos \psi) \right\} \cos \psi \\ &= \frac{J_0(|\bar{\mathbf{l}}|) - J_2(|\bar{\mathbf{l}}|)}{2} \cos^2 \gamma_m \cos^2 \psi \\ &\quad + \frac{J_1(|\bar{\mathbf{l}}|)}{|\bar{\mathbf{l}}|} \sin^2 \gamma_m \cos \psi. \end{aligned} \quad (49)$$

Finally, it follows from (41) that

$$\begin{aligned} T_{14} &= T_{11} \sin \psi \\ T_{(i+1)4} &= T_{1(i+1)} \sin \psi \\ T_{44} &= T_{11} \sin^2 \psi. \end{aligned} \quad (50)$$

## APPENDIX B

$$M \triangleq \frac{1}{4\pi} \int_{\mathcal{U}} e^{j\mathbf{u}^T \mathbf{l}} \begin{bmatrix} 1 \\ \mathbf{u} \end{bmatrix} [1 \quad \mathbf{u}^T] d\mathbf{u}. \quad (51)$$

Denoting the angle between  $\mathbf{d}$  and  $\mathbf{u}$  by  $\gamma$ , we can write the upper left entry of the  $4 \times 4$  matrix  $M$  as

$$M_{11} = \frac{1}{4\pi} \int_{\mathcal{U}} e^{i|\mathbf{l}| \cos \gamma} d\mathbf{u} = j_0(|\mathbf{l}|). \quad (52)$$

Following similar reasoning that used in Appendix A, the remaining entries of the first row and column of  $M$  are

$$\begin{aligned} M_{(m+1)1} &= M_{1(m+1)} = \frac{-i}{4\pi} \int_{\mathcal{U}} \frac{\partial}{\partial l_m} \exp^{i\mathbf{u}^T \mathbf{l}} d\mathbf{u} \\ &= -i \frac{\partial}{\partial l_m} M_{11} \end{aligned} \quad (53)$$

for  $m = 1, 2, 3$ , and the lower  $3 \times 3$  block of  $M$  has entries

$$M_{(m+1)(n+1)} = -\frac{\partial^2}{\partial l_m \partial l_n} M_{11} \quad (54)$$

for  $m, n = 1, 2, 3$ . Using a certain recurrence relationship between the spherical Bessel functions [32, p. 622],  $d(x^{-n} j_n(x))/dx = -x^{-n} j_{n+1}(x)$ , the partial derivatives can be evaluated

$$M_{(m+1)1} = M_{1(m+1)} = -i \frac{l_m}{|\bar{\mathbf{l}}|} j_0^{(1)}(|\mathbf{l}|) = i j_1(|\mathbf{l}|) \cos \gamma_m. \quad (55)$$

When  $m \neq n$

$$\begin{aligned} M_{(m+1)(n+1)} &= l_m \frac{\partial}{\partial l_n} \frac{j_1(|\mathbf{l}|)}{|\mathbf{l}|} = -\frac{l_m l_n}{|\mathbf{l}|} \frac{j_2(|\mathbf{l}|)}{|\mathbf{l}|} \\ &= -j_2(|\mathbf{l}|) \cos \gamma_m \cos \gamma_n \end{aligned} \quad (56)$$

and

$$\begin{aligned} M_{(m+1)(m+1)} &= \frac{\partial}{\partial l_m} \frac{l_m}{|\mathbf{l}|} j_1(|\mathbf{l}|) = \frac{j_1(|\mathbf{l}|)}{|\mathbf{l}|} - \frac{l_m^2}{|\mathbf{l}|} \frac{j_2(|\mathbf{l}|)}{|\mathbf{l}|} \\ &= \frac{j_1(|\mathbf{l}|)}{|\mathbf{l}|} - j_2(|\mathbf{l}|) \cos^2 \gamma_m. \end{aligned} \quad (57)$$

## REFERENCES

- [1] A. Nehorai and E. Paldi, "Acoustic vector-sensor array processing," in *Proc. 26th Asilomar Conf. Signals, Systems and Computers*, Pacific Grove, CA, Oct. 1992, pp. 192–198.
- [2] —, "Acoustic vector-sensor array processing," *IEEE Trans. Signal Processing*, vol. 42, pp. 2481–2491, Sept. 1994.
- [3] M. Hawkes and A. Nehorai, "Acoustic vector-sensor beamforming and Capon direction estimation," *IEEE Trans. Signal Processing*, vol. 46, pp. 2291–2304, Sept. 1998.

- [4] —, "Effects of sensor placement on acoustic vector-sensor array performance," *IEEE J. Oceanic Eng.*, vol. 24, pp. 33–40, Jan. 1999.
- [5] —, "Acoustic vector-sensor processing in the presence of a reflecting boundary," *IEEE Trans. Signal Processing*.
- [6] M. J. Berliner and J. F. Lindberg, Eds., *Acoustic Particle Velocity Sensors: Design, Performance and Applications*. Woodbury, NY: AIP, 1996.
- [7] J. C. Nickles *et al.*, "A vertical array of directional acoustic sensors," in *Proc. Oceans '92*, Newport, RI, Oct. 1992, pp. 340–345.
- [8] G. L. D'Spain *et al.*, "Initial analysis of the data from the vertical DIFAR array," in *Proc. Oceans '92*, Newport, RI, Oct. 1992, pp. 346–351.
- [9] K. T. Wong and M. D. Zoltowski, "Closed-form underwater acoustic direction-finding with arbitrarily spaced vector hydrophones at unknown locations," *IEEE J. Oceanic Eng.*, vol. 22, pp. 566–575, July 1997.
- [10] —, "Extended-aperture underwater acoustic multisource azimuth/elevation direction-finding using uniformly but sparsely-spaced vector hydrophones," *IEEE J. Oceanic Eng.*, vol. 22, pp. 659–672, Oct. 1997.
- [11] —, "Root-MUSIC-based azimuth-elevation angle-of-arrival estimation with uniformly spaced but arbitrarily oriented velocity hydrophones," *IEEE Trans. Signal Processing*, vol. 47, pp. 3250–3260, Dec. 1999.
- [12] —, "Self-initiating MUSIC-based direction finding in underwater acoustic particle velocity-field beamspace," *IEEE J. Oceanic Eng.*, vol. 25, pp. 262–273, Apr. 2000.
- [13] A. Paulraj, B. Ottersten, R. Roy, A. Swindlehurst, G. Xu, and T. Kailath, "Subspace methods for directions-of-arrival estimation," in *Handbook of Statistics*, N. Bose and C. Rao, Eds. Amsterdam, The Netherlands: Elsevier, 1993, vol. 10, pp. 693–739.
- [14] B. Goransson and B. Ottersten, "Direction estimation in partially unknown noise fields," *IEEE Trans. Signal Processing*, vol. 47, pp. 2375–2385, Sept. 1999.
- [15] B. Friedlander and A. J. Weiss, "Direction finding using noise covariance modeling," *IEEE Trans. Signal Processing*, vol. 43, pp. 1557–1567, July 1995.
- [16] B. F. Cron and C. H. Sherman, "Spatial-correlation functions for various noise models," *J. Acoust. Soc. Amer.*, vol. 34, pp. 1732–1736, 1962.
- [17] W. S. Liggett and J. Jacobson, "Covariance of surface-generated noise in a deep ocean," *J. Acoust. Soc. Amer.*, vol. 38, no. 1, pp. 303–311, 1966.
- [18] W. A. Kuperman and F. Ingenito, "Spatial correlation of surface generated noise in a stratified ocean," *J. Acoust. Soc. Amer.*, vol. 67, no. 6, pp. 198–1996, 1980.
- [19] H. Cox, "Spatial correlation in arbitrary noise fields with application to ambient sea noise," *J. Acoust. Soc. Amer.*, vol. 54, pp. 1289–1301, 1973.
- [20] M. J. Buckingham, "A theoretical noise model of ambient noise in a low-loss shallow water channel," *J. Acoust. Soc. Amer.*, vol. 67, no. 4, pp. 1186–1192, 1980.
- [21] R. J. Talham, "Noise correlation functions for anisotropic noise fields," *J. Acoust. Soc. Amer.*, vol. 69, no. 1, pp. 213–215, 1981.
- [22] R. Kneipfer, "Spatial auto and cross-correlation functions for tri-axial velocity sensor outputs in a narrowband, 3 dimensional, isotropic pressure field," Naval Undersea Warfare Center Division, Newport, RI, NUWC Memo. 5214/87, Sept. 1995.
- [23] B. A. Cray and A. H. Nuttall, "A comparison of vector-sensing and scalar-sensing linear arrays," Naval Undersea Warfare Center Division, Newport, RI, NUWC-NPT Tech. Rep., no. 10 632, Jan. 1997.
- [24] A. D. Pierce, *Acoustics: An Introduction to its Physical Principles and Applications*. New York: McGraw-Hill, 1981.
- [25] H. Cox, "Fundamentals of bistatic active sonar," in *Proc. NATO Advanced Study Inst. Underwater Acoustic Data Process.*, Y. T. Chan, Ed. Norwood, MA: Kluwer, 1989.
- [26] S. Haykin, *Communications Systems*, 2nd ed. New York: Wiley, 1983.
- [27] E. L. Lehmann, *Theory of Point Estimation*. New York: Wiley, 1983.
- [28] S. M. Kay, *Fundamentals of Statistical Signal Processing: Estimation Theory*. Englewood Cliffs, NJ: Prentice-Hall, 1993.
- [29] A. Nehorai and M. Hawkes, "Performance bounds for estimating vector systems," *IEEE Trans. Signal Processing*, vol. 48, June 2000.
- [30] V. H. MacDonald and P. M. Schultheiss, "Optimum passive bearing estimation in a spatially incoherent noise environment," *J. Acoust. Soc. Amer.*, vol. 46, pp. 37–43, 1969.
- [31] W. H. Breyer, *CRC Standard Mathematical Tables*, 28th ed. Boca Raton, FL: CRC Press, 1987.
- [32] P. M. Morse and H. Feshbach, *Methods of Theoretical Physics: Part I*. New York: McGraw-Hill, 1953.

**Malcolm Hawkes** (S'95–M'00) was born in Stockton-on-Tees, U.K., in 1970. He received the B.A. degree in electrical and information science from the University of Cambridge, Cambridge, U.K., the M.Sc. degree in applied statistics from the University of Oxford, Oxford, U.K., and the Ph.D. degree in electrical engineering from Yale University, New Haven, CT, in 1992, 1993, and 2000, respectively.

In 1988, he won a scholarship from GEC-Marconi Research Centre, Chelmsford, U.K., and worked there from 1988 to 1989, and again in the summers of 1990 and 1991. From 1996 to 2000, he was a Visiting Scholar at the University of Illinois, Chicago. He is now a Research Associate with Stafford Trading, Inc. in Chicago, IL. His research interests include statistical signal processing and time series analysis with applications in finance, array processing, and biomedicine.

Dr. Hawkes won scholarships at Emmanuel College, University of Cambridge, in 1990, 1991, and 1992, was awarded a U.K. Medical Research Council grant to pursue a Master's program in 1992, and a Yale University Fellowship in 1993, and received the John and Grace Nuveen International Scholar Award from the University of Illinois, Chicago, in 1998.

**Arye Nehorai** (S'80–M'83–SM'90–F'94) received the B.Sc. and M.Sc. degrees in electrical engineering from the Technion–Israel Institute of Technology, Israel, in 1976 and 1979, respectively, and the Ph.D. degree in electrical engineering from Stanford University, Stanford, CA, in 1983.

After graduation, he worked as a Research Engineer for Systems Control Technology, Inc., in Palo Alto, CA. From 1985 to 1995, he was with the Department of Electrical Engineering at Yale University, New Haven, CT, where he became an Associate Professor in 1989. In 1995, he joined the Department of Electrical Engineering and Computer Science at The University of Illinois at Chicago (UIC), as a Full Professor. He holds a joint professorship with the Bioengineering Department at UIC. His research interests are in signal processing, communications, and biomedicine.

Dr. Nehorai is a member of the Editorial Board of *Signal Processing*, has served as Chairman of the Connecticut IEEE Signal Processing Chapter from 1986 to 1995, is a founding member, and current Chair, of the IEEE Signal Processing Society's Technical Committee on Sensor Array and Multichannel (SAM) Processing, and was the co-General Chair of the *First IEEE SAM Signal Processing Workshop* in March 2000. He is Editor-in-Chief of the IEEE TRANSACTIONS ON SIGNAL PROCESSING, an Associate Editor of *Circuits, Systems, and Signal Processing*, and *The Journal of the Franklin Institute*, and has previously been an Associate Editor of the IEEE TRANSACTIONS ON ACOUSTICS, SPEECH AND SIGNAL PROCESSING, of IEEE SIGNAL PROCESSING LETTERS, IEEE TRANSACTIONS ON ANTENNAS AND PROPAGATION, and IEEE JOURNAL OF OCEANIC ENGINEERING. He has been a Fellow of the Royal Statistical Society since 1996. He was co-recipient, with P. Stoica, of the 1989 IEEE Signal Processing Society's Senior Award for Best Paper.